3D Printed Flexible Photoplethysmography Sensor Array for Tissue Oximetry

Matas Petreikis, Manish K Tiwari
Nanoengineered Systems Laboratory, UCL Mechanical Engineering, London, UK
Wellcome/EPSRC Centre for Interventional and Surgical Sciences, UCL, London, UK

zcicmpe@ucl.ac.uk, m.tiwari@ucl.ac.uk

***Abstract*—Recently there has been a trend to use the optoelectronic system of pulse oximeters, a photodiode and a pair of light emitting diodes of different wavelengths, to perform elementary tissue oximetry by measuring the changes in oxygenated and deoxygenated haemoglobin concentrations in tissues. This paper presents introductory work into how an affordable flexible array of such tissue oximeters could be manufactured by using direct-write 3D printing and commercial surface mount devices. For this purpose, a flexible printed circuit board was fabricated by printing 30 wt. % silver nanoparticle ink on 60 µm polyimide film. An array of photoplethysmography (PPG) sensors was made by combining the circuit board with two pairs of 660 nm and 940 nm light emitting diodes and six photodiodes. It was demonstrated how this combination of optoelectronic devices results in a 2-by-4 array of PPG sensors with capability to simultaneously measure PPG signals with multiple photodiodes. It was concluded that further work must be completed to evaluate the possibility of this sensor array to be used for tissue oximetry.**

Keywords—flexible; 3D printing; photoplethysmography; oximetry

I. INTRODUCTION

Development and fabrication of flexible and wearable sensors for medicine, e.g. temperature [1, 2], pressure [3-5], blood oxygen [6-9] measurements, sweat analysis [10-14], have become increasingly more common both in research and commercial settings in the last ten years. Wearable and flexible body sensors offer multiple advantages over their non-wearable counterparts, including potentially improved performance due to their better conformability to the individual's skin [7], easier integration of multiple different sensors in a single device [13, 15] and improved ergonomics, as well as cheaper and quicker health problem detection [16, 17] due to the continuous unobtrusive health monitoring. Naturally, blood oxygen sensors, typically measuring the saturation of oxygenated haemoglobin (HbO_2) in pulsatile blood, denoted as S_pO_2, have not been an exception and numerous devices, from commercially available smartwatches [9] to miniaturized wearable S_pO_2 sensors [6, 8], have been shown, demonstrating the increased use of continuous blood oxygen monitoring for years to come.

Nevertheless, a novel use of such and similar S_pO_2 sensors has been proposed by measuring the changes in concentrations of oxygenated and deoxygenated haemoglobin (HHb) in tissues, i.e. $\Delta[HbO_2]$ and $\Delta[HHb]$, respectively [7, 15, 18-20]. The ability to measure those changes not only in pulsatile blood, which usually is composed of only arterial blood, but in all of the blood in tissues is the quality that enables the use of such devices for monitoring of injured tissues, such as after reconstructive surgeries or with chronic wounds [7, 20, 21]. Consequently, these devices have been proposed as an alternative to more expensive and cumbersome sensors that are commonly used for such applications, e.g. implantable and non-implantable laser Doppler devices [21].

The reason why S_pO_2 sensors can be employed to perform $\Delta[HbO_2]$ and $\Delta[HHb]$ measurements, i.e. indirect tissue oximetry, lies within the methodology of pulse oximetry. According to Beer-Lambert's law [7], S_pO_2 can be calculated as follows

$$S_pO_2 = \frac{\varepsilon_{HHb}(\lambda_1) - \varepsilon_{HHb}(\lambda_2)\, R'_{os}}{(\varepsilon_{HHb}(\lambda_1) - \varepsilon_{HbO2}(\lambda_1)) + (\varepsilon_{HbO2}(\lambda_2) - \varepsilon_{HHb}(\lambda_2))\, R'_{os}} \quad (1)$$

where $\varepsilon_{HHb}(\lambda)$ and $\varepsilon_{HbO2}(\lambda)$ are the molar extinction coefficients of deoxygenated and oxygenated haemoglobin as functions of the wavelength of the light absorbed, respectively, and R'_{os} is the modified modulation ratio. R'_{os} is the product of the modulation ratio R_{os}, which can be determined from the PPG signal detected using two wavelengths λ_1 and λ_2, and the ratio between the differential pathlength factors for those two wavelengths ($DPF(\lambda_2)/DPF(\lambda_1)$) [7]. The values for those factors are usually taken from the literature [6, 15]. However, $DPF(\lambda_1)$ and $DPF(\lambda_2)$ can be used to perform $\Delta[HbO_2]$ and $\Delta[HHb]$ measurements as shown in (2) [7]

$$\begin{bmatrix} \varepsilon_{HbO2}(\lambda_1) & \varepsilon_{HHb}(\lambda_1) \\ \varepsilon_{HbO2}(\lambda_2) & \varepsilon_{HHb}(\lambda_2) \end{bmatrix} \begin{bmatrix} \Delta[HbO_2] \\ \Delta[HHb] \end{bmatrix} = \begin{bmatrix} \dfrac{\ln \frac{I_0(\lambda_1)}{\Delta I(\lambda_1)}}{d\, DPF(\lambda_1)} \\ \dfrac{\ln \frac{I_0(\lambda_2)}{\Delta I(\lambda_2)}}{d\, DPF(\lambda_2)} \end{bmatrix} \quad (2)$$

where $I_0(\lambda)$ is a baseline wavelength-specific photocurrent generated, $\Delta I(\lambda)$ is the corresponding change in the photocurrent level with respect to the baseline, and d is the light source to photodetector distance.

Here we improve upon the previously developed sensors by demonstrating the fabrication of an array of PPG sensors, which could in the future be used for indirect tissue oximetry, using direct-write 3D printing [22-25] and by employing commercially available light-emitting diodes (LEDs) and photodiodes (PDs). This method of fabrication

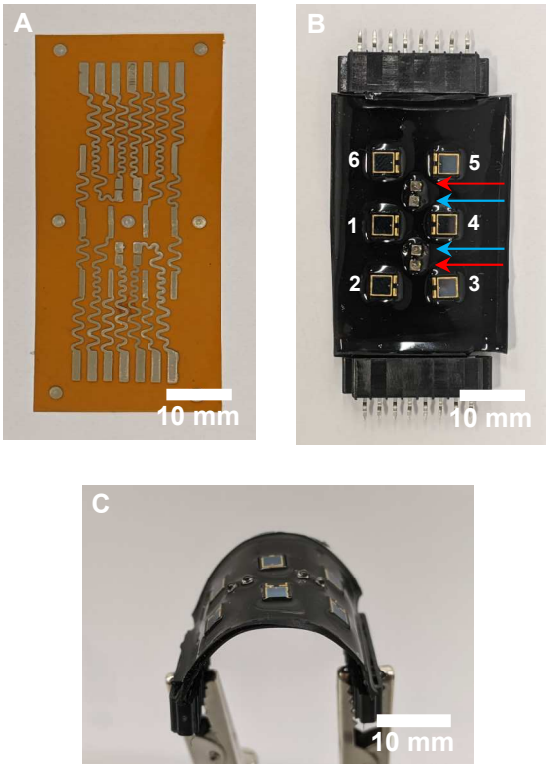

Fig. 1 (A) A flexible printed circuit board (FPCB) printed and used for the fabrication of the sensor, (B) a fully fabricated array of pulse oximetry sensors with red and blue arrows pointing at 660 nm and 940 nm LEDs, respectively, (C) demonstrating the flexibility of the pulse oximetry array by bending it with a radius of curvature of approximately 14 mm.

was chosen to reflect the need for rapid customization of the shape of the sensor for its application in monitoring of injured tissues and its relatively low cost even when manufactured at low volumes.

II. Methods

A. Sensor Fabrication

Flexible printed circuit boards (FPCBs) were prepared by direct-write printing of silver interconnects using 30 wt. % silver nanoparticle dispersion in ethylene glycol (Sigma-Aldrich) onto 60 µm polyimide (PI) sheets using 102 µm nozzle (32 GA, Metcal). The printed pattern was designed using Autodesk Eagle and the generated Gerber file was then converted to G-code using FlatCAM. Prior to printing, the PI substrates were prepared by rinsing them in acetone, isopropyl alcohol, and deionised (DI) water, followed by 5 min oxygen plasma treatment and a subsequent rinse in DI water. The silver nanoparticle ink used in this work had a sufficiently low viscosity (28 cP), therefore, no overpressure was needed for its extrusion when using the 102 µm nozzles. Nanopositioning stages (Aerotech Nanopositioner ANT130L) employed in the 3D printing system allow for a 4 cm × 4 cm size prints; in this case, each FPCB was prepared by performing two side-by-side prints. Multipass printing with five layers of ink enabled lower interconnect resistance. The printed interconnect patterns were then cured at 240 °C for 4 hours. Optoelectronic components, i.e. PDs, 660 nm and 940 nm LEDs, were integrated onto the substrates by using a two-part conductive epoxy (MG Chemicals) and curing the samples at 65 °C for 2 hours. After that, the FPCBs were encapsulated by carefully applying Ecoflex (Dragon Skin™ 30), which was dyed using up to 2 wt. % of

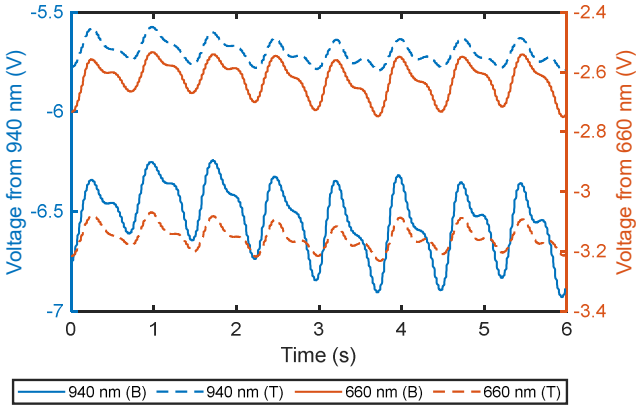

Fig. 2 PPG signals recorded by PD no. 1 from four LEDs simultaneously when an index finger is placed on the PD and the four LEDs at the same time. B and T letters are assigned in order to distinguish from which pair of LEDs, bottom (B) or top (T), the PPG is signals are recorded.

carbon black powder, over the interconnects and other areas of the FPCBs but not covering the LEDs and PDs. Dyed Ecoflex was used as we found that the sensor performance in terms of the ratio of AC to DC signal from the PPG waveforms, which were recorded using 940 nm light, improved in comparison to the performance of sensors with translucent Ecoflex encapsulation. Similar strategy to reduce the negative effect from the ambient light has been reported before [15]. The concentration of carbon black in Ecoflex used was not great enough to result in a conductive encapsulation layer, consequently, no short circuits were formed by performing the encapsulation of the sensor array in this way.

B. Signal Acquisition and Processing

The LEDs were biased and the photocurrent from the PDs was collected by inserting ends of the FPCBs into connectors and subsequently connecting them to either an Arduino Uno board with MCP4728 DAC for the LED biasing or a separate amplification circuit for the photocurrent, which was then recorded using an oscilloscope. 660 nm and 940 nm LEDs were sequentially biased at 5.40 V and 1.35 V, respectively, at 50 Hz frequency with 25 % duty cycle. The output from each PD was amplified with an individual inverting transimpedance amplifier, with a gain of 2.2×10^6. The PDs were reverse biased with 0.5 V voltage when the sensor was operating to ensure their stable operation and constant responsivity. The amplified signal from each PD was filtered by using a 10th order lowpass Butterworth filter with 3 Hz cut-off frequency.

III. Results and Discussion

A. Sensor Fabrication

As it can be seen from Fig. 1 (A) and (B), in which a 3D-printed pattern of the FPCB is shown, the sensor was designed to have 6 PDs and two pairs of 660 nm and 940 nm LEDs with the distance between the centre points in between the pairs of LEDs and each neighbouring PD to be 7 mm. The interconnects were arranged in serpentine-like shapes in order to increase the flexibility of the FPCB and prevent their cracking during bending. Five layers of silver ink were deposited for each FPCB in order to minimise the probability of critical flaws in the print as well as to reduce the resistance of each interconnect. Interconnect resistance for FPCBs used for the experiments presented here varied from 2.5 ± 0.8 Ω to

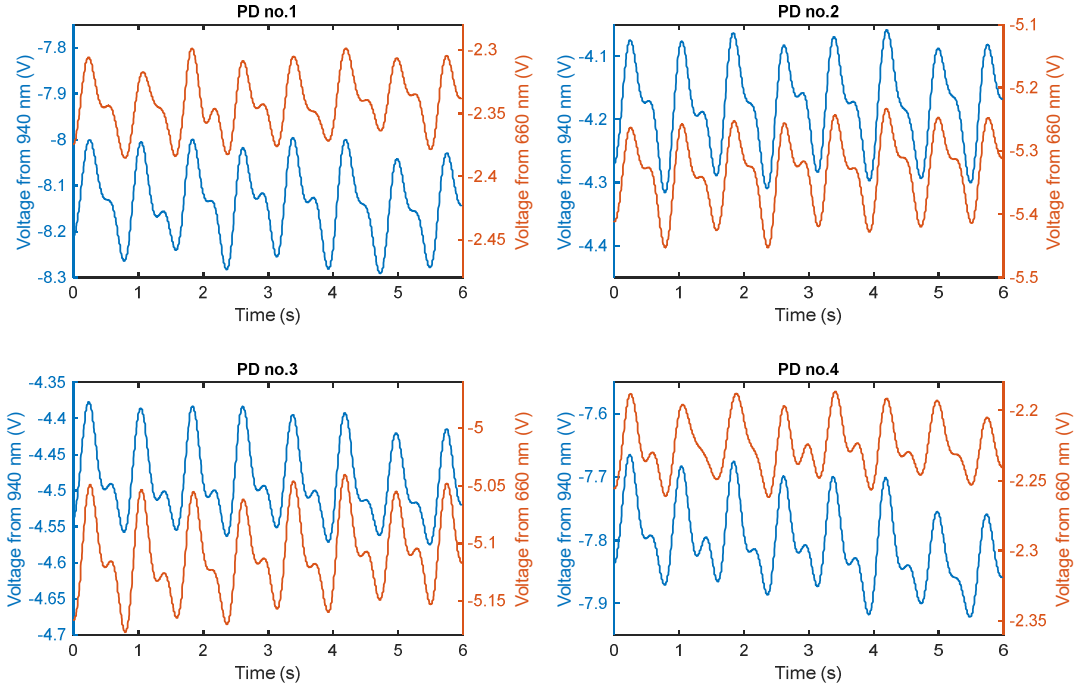

Fig. 3 Simultaneous PPG signals recorded when a thumb was placed to cover the bottom 660 nm and 940 nm LEDs and PDs 1 to 4.

9.3 ± 1.4 Ω, having measured the resistances of four interconnects of each geometry on the FPCB. Following the mounting of the optoelectronic components onto the FPCB, the sensor was encapsulated in dyed Ecoflex as it is shown in Fig. 1 (B). Fig. 1 (C) shows how the fully fabricated sensor can easily undergo bending with a curvature of radius of 14 nm. With the intended sensor application in mind, i.e. the monitoring of injured skin tissue, we believe the sensor array is sufficiently flexible as any deformation with a smaller radius of curvature is unlikely.

B. Separating PPG Signals

When biasing the LEDs on the sensor array, it was essential to ensure that the PPG signal from each LED could be distinguished from the overall output of each PD. The selected voltages in conjunction with different molar extinction coefficients of 660 nm and 940 nm light by the tissue as well as slightly different resistances of the interconnects resulted in different DC levels of the photocurrent recorded. For example, Fig. 2 shows the four different PPG signals recorded when PD 1 and the four LEDs are covered with an index finger. The DC values of the signals were sufficiently different that they could be easily distinguished from the overall output of PD 1; the same result was achieved when testing PD 4. Therefore, PD 1 and PD 4 each create two PPG sensors with the neighbouring LEDs. All the other PDs on the array were confirmed to be able to detect two PPG signals, i.e. for 660 nm and 940 nm light. In total these findings show that this sensor array is capable of 2 × 4 PPG recordings for two wavelengths of light.

C. Simultaneous PPG Measurements

Fig. 3 shows how multiple PDs, in this case four of them, can record two PPG waveforms each simultaneously when a thumb is placed on those optoelectronic components. The waveforms for 660 nm light recorded by PDs 1 and 4 have smaller AC and DC signal magnitudes than the equivalent 940 nm waveforms. On the other hand, the signals recorded by PDs 2 and 3 have higher DC magnitudes for 660 nm light while the AC signal for both wavelengths is of a similar amplitude. The differences in DC signal magnitudes can be explained by the fact that the 940 nm LED is closer to PDs 1 and 4 than the 660 nm LED, and vice versa for PDs 2 and 3; and the fact that the intensity of scattered light reflecting off the skin decreases exponentially with the distance from the light source [26]. Regarding the AC magnitude, it can be evaluated as a ratio to the DC value because a relatively low ratio would indicate that a low fraction of light is absorbed by the pulsatile blood which is undesirable in a PPG or an S_pO_2 sensor. In the recordings in Fig. 3, the ratio of the AC to DC signal, having considered the additional -0.5 V DC offset due to the reverse bias of the PD, for 660 nm and 940 nm light was in the range of 0.02 – 0.03 and 0.02 – 0.05, respectively. These values agree with results that have been shown before with non-3D-printed sensors in [6, 7, 26, 27]. Despite the promising results, the sensor array calibration based on (1) and attempts to perform $\Delta[HbO_2]$ and $\Delta[HHb]$ measurements as described in (2) should be achieved in the future in order to assess the viability of this device to be used as a tissue oximeter.

IV. Conclusions

Here we demonstrated how an affordable flexible array of PPG sensors could be fabricated by employing direct-write 3D printing of 30 wt. % silver nanoparticle ink on polyimide substrate and using commercially available surface mount devices, i.e., 660 nm and 940 nm LEDs and photodiodes. It was demonstrated that a combination of six PDs and two pairs of LEDs can produce a 2 × 4 PPG sensor array, which is capable of simultaneously detecting PPG waveforms for both 660 nm and 940 nm wavelengths with multiple PDs.

REFERENCES

[1] Trung TQ, Ramasundaram S, Hwang BU, Lee NE. An all-elastomeric transparent and stretchable temperature sensor for body-attachable wearable electronics. Advanced materials. 2016 Jan;28(3):502-9.

[2] Yang J et al. Wearable temperature sensor based on graphene nanowalls. Rsc Advances. 2015;5(32):25609-15.

[3] Gong S et al. A wearable and highly sensitive pressure sensor with ultrathin gold nanowires. Nature communications. 2014 Feb 4;5(1):1-8.

[4] Kwak JW et al. Wireless sensors for continuous, multimodal measurements at the skin interface with lower limb prostheses. Science translational medicine. 2020 Dec 16;12(574):eabc4327.

[5] Trung TQ, Lee NE. Flexible and stretchable physical sensor integrated platforms for wearable human-activity monitoringand personal healthcare. Advanced materials. 2016 Jun;28(22):4338-72.

[6] Kim J et al. Miniaturized battery-free wireless systems for wearable pulse oximetry. Advanced functional materials. 2017 Jan;27(1):1604373.

[7] Khan Y et al. A flexible organic reflectance oximeter array. Proceedings of the National Academy of Sciences. 2018 Nov 20;115(47):E11015-24.

[8] Yokota T et al. Ultraflexible organic photonic skin. Science advances. 2016 Apr 15;2(4):e1501856.

[9] Pipek LZ, Nascimento RF, Acencio MM, Teixeira LR. Comparison of SpO2 and heart rate values on Apple Watch and conventional commercial oximeters devices in patients with lung disease. Scientific Reports. 2021 Sep 23;11(1):1-7.

[10] Koh A et al. A soft, wearable microfluidic device for the capture, storage, and colorimetric sensing of sweat. Science translational medicine. 2016 Nov 23;8(366):366ra165-.

[11] Ghaffari R et al. Soft wearable systems for colorimetric and electrochemical analysis of biofluids. Advanced Functional Materials. 2020 Sep;30(37):1907269.

[12] Anastasova S et al. A wearable multisensing patch for continuous sweat monitoring. Biosensors and Bioelectronics. 2017 Jul 15;93:139-45.

[13] Gao W et al. Fully integrated wearable sensor arrays for multiplexed in situ perspiration analysis. Nature. 2016 Jan;529(7587):509-14.

[14] Nyein HY et al. Regional and correlative sweat analysis using high-throughput microfluidic sensing patches toward decoding sweat. Science advances. 2019 Aug 16;5(8):eaaw9906.

[15] Kim J et al. Battery-free, stretchable optoelectronic systems for wireless optical characterization of the skin. Science advances. 2016 Aug 3;2(8):e1600418.

[16] Kristoffersson A, Lindén M. A systematic review on the use of wearable body sensors for health monitoring: a qualitative synthesis. Sensors. 2020 Jan;20(5):1502.

[17] Mukhopadhyay SC. Wearable sensors for human activity monitoring: A review. IEEE sensors journal. 2014 Dec 4;15(3):1321-30.

[18] Zhang H et al. Wireless, battery-free optoelectronic systems as subdermal implants for local tissue oximetry. Science advances. 2019 Mar 8;5(3):eaaw0873.

[19] Kang MH et al. Outdoor-Useable, Wireless/Battery-Free Patch-Type Tissue Oximeter with Radiative Cooling. Advanced Science. 2021 May;8(10):2004885.

[20] Simone G et al. High-Accuracy Photoplethysmography Array Using Near-Infrared Organic Photodiodes with Ultralow Dark Current. Advanced Optical Materials. 2020 May;8(10):1901989.

[21] Chen CM, Kwasnicki RM, Curto VF, Yang GZ, Lo BP. Tissue oxygenation sensor and an active in vitro phantom for sensor validation. IEEE Sensors Journal. 2019 May 15;19(18):8233-40.

[22] Ahn BY et al. Omnidirectional printing of flexible, stretchable, and spanning silver microelectrodes. Science. 2009 Mar 20;323(5921):1590-3.

[23] Ahn BY et al. Planar and three-dimensional printing of conductive inks. JoVE (Journal of Visualized Experiments). 2011 Dec 9(58):e3189.

[24] Walker SB, Lewis JA. Reactive silver inks for patterning high-conductivity features at mild temperatures. Journal of the American Chemical Society. 2012 Jan 25;134(3):1419-21.

[25] Fang F, Aabith S, Homer-Vanniasinkam S, Tiwari MK. High-resolution 3D printing for healthcare underpinned by small-scale fluidics. In3D Printing in Medicine 2017 Jan 1 (pp. 167-206). Woodhead Publishing.

[26] Lee H et al. Organic–Inorganic Hybrid Approach to Pulse Oximetry Sensors with Reliability and Low Power Consumption. ACS Photonics. 2021 Nov 16;8(12):3564-72.

[27] Lee H et al. Toward all-day wearable health monitoring: An ultralow-power, reflective organic pulse oximetry sensing patch. Science advances. 2018 Nov 9;4(11):eaas9530.